Dimensional signature on noise-induced excitable statistics in an optically injected semiconductor laser

B. Kelleher,[1,2] D. Goulding,[2,3] G. Huyet,[1,2] E. A. Viktorov,[1,4] T. Erneux,[4] and S. P. Hegarty[1,2]

[1]*Centre for Applied Photonics and Process Analysis, Cork Institute of Technology, Cork, Ireland*

[2]*Tyndall National Institute, Lee Maltings, Cork, Ireland*

[3]*Department of Physics, University College Cork, Cork, Ireland*

[4]*Optique Nonlinéaire Théorique, Université Libre de Bruxelles, Campus Plaine, Code Postal 231, B-1050 Bruxelles, Belgium*

(Received 14 May 2010; revised manuscript received 14 June 2011; published 29 August 2011)

Noise-induced excitability is a prevalent feature in many nonlinear dynamical systems. The optically injected semiconductor laser is one of the simplest such systems and is readily amenable to both experimental and theoretical analysis. We show that the dimensionality of this system may be tuned experimentally and that this has a strong signature on the interspike statistics. The phase of the slave laser is resolved experimentally in the frame of the master laser, allowing an examination of the dynamics at extremely low injection strengths where intensity measurements alone cannot determine the dynamics fully. Generic phase equations are found for the different dimensional scenarios. When the dimensionality is greater than 1, we show that a precursor of a homoclinic bifurcation generates a noise-induced frequency and that the homoclinic bifurcation admits a bistability in the system.

DOI: 10.1103/PhysRevE.84.026208 PACS number(s): 05.45.Xt, 05.40.Ca, 42.55.Px, 42.65.Sf

I. INTRODUCTION

Noise-induced phenomena are of considerable importance in all areas of science and technology. The presence of noise in some systems results in excitability, a feature common to many areas of study. It was originally introduced in a biological setting in [1] and has since been studied in many different fields [2] and, most importantly for this work, in systems of semiconductor lasers [3–9]. A system is excitable if there exists a stable equilibrium and a perturbation threshold beyond which a large phase space trajectory back to the stable point results, typically associated with an amplitude pulsation. (These excitations are commonly referred to as spikes.) A deep feature of the effect of noise in excitable systems is coherence resonance, a phenomenon that typically involves the appearance of noise-induced frequencies even when the system does not have any intrinsic deterministic frequency [10–13], often resulting from noise-induced diffusion out of a potential minimum. The seminal work on noise-induced escape from potential minima is that of Kramers [14,15], who showed that the probability of escape was governed by an exponential decay with a characteristic time depending on the noise strength (explaining at the same time the empirical Arrhenius activation law). An important class of such potentials is the class of tilted potentials [16], and these have relevance in many physical systems, such as Josephson junctions, superconductors, neuronal processes, coupled electrical oscillators, and coupled lasers,among others. We consider here one of the most important coupled laser configurations: that of the optically injected laser. This system is of interest to researchers in diverse fields because of its relative experimental simplicity and, conversely, the rich dynamical behavior observed, including synchronization, excitability, multistability, and chaos [17]. What's more, much of the underlying physics can be described via the Adler model [18], one of the prototype tilted potential models, first derived for the phase coupling of electrical oscillators. For very low injection strengths, the optically injected system should be well approximated by the Adler model [19]. In this approximation one should observe 2π phase rotations in the presence of noise manifest as excitable intensity spikes or pulsations [2,7], and the distribution of the interspike times is predicted to be an exponential decay [10]. However, for the very low injection strengths where it is expected to give the most accurate description, the intensity changes are very small compared to the free-running intensity, and for sufficiently low levels, the pulsations can be (at least partially) masked by the noise in the system and thus cannot be identified unambiguously in an intensity time series. As a result, the excitable properties of the optically injected laser have never been systematically tested experimentally in this limit. For higher injection strengths both the intensity and the carrier density of the locked slave electric field can differ significantly from the free-running intensity and carrier density, and the intensity pulsations are easily observed [7].

In this work we use a recently developed experimental method to resolve the phase of the slave laser at any injection strength. This allows an analysis of the dynamics at extremely low injection levels and thus the identification of excitable events, even where noise hides the intensity pulsations. This permits a direct analysis of the ability of the Adler model to provide an accurate description of the system, and we verify experimentally the exponential distribution. For moderate injection strengths where the pulsations are easily visible above the noise, we again measure the interspike times and demonstrate a region of nonexponential behavior, indicating that the system is no longer accurately modeled by the Adler equation. We measure the phasor of the slave undergoing excitable pulsations in this region and show how it differs significantly from that at low injection levels. Starting from the standard quantum dot rate equations, we derive a third-order phase model for the system, generalizing the Adler equation. From this we uncover the theoretical explanation of the nonexponential behavior and display an excellent agreement between numerical simulations and the

experiment. We also show how a dimensional reduction leads to a second-order phase model formally identical to the forced nonlinear pendulum. Finally, we show how the results correlate with the Fokker-Planck potential approach.

II. OPTICAL INJECTION AND THE ADLER MODEL

For low injection levels the optically injected system should be well approximated by the Adler model, as shown in [19]. The Adler model is a one-dimensional system with the governing equation given by

$$\dot{\phi} = -\Delta - \kappa\sqrt{1+\alpha^2}\,\sin(\phi + \phi_0), \qquad (1)$$

where ϕ is the phase of the slave in the frame of the master, Δ is the detuning (the angular frequency of the master minus that of the slave), κ is a measure of the coupling strength, α is the linewidth enhancement factor, and $\phi_0 = \arctan\alpha$. (Note that this can be rewritten in the usual Adler form as $\psi = -\Delta - \eta\sin\psi$ by defining $\psi = \phi + \phi_0$ and $\eta = \kappa\sqrt{1+\alpha^2}$.) If $|\Delta| < \kappa\sqrt{1+\alpha^2}$, the slave can be phase locked to the master so that its frequency equals that of the master and it has a fixed relative phase. The locking boundary at $|\Delta| = \kappa\sqrt{1+\alpha^2}$ is a saddle-node infinite-period bifurcation [20], where a pair of equilibria, one stable (the node) and one unstable (the saddle), are born. Phase-locked behavior consists of the system residing at the stable point. Outside the locking region, the phase is unbounded. In the phasor-like representation ($\cos\phi$,$\sin\phi$), this unbounded, running-phase solution is periodic, and far from the locking boundary it corresponds to the frequency beating of the two oscillators. The period of this solution becomes infinite at the locking boundary. Within the locking region and in the presence of noise, the phase jiggles around the stable point, and if it passes the unstable point, then a rotation back to the stable point results (giving a 2π rotation in total). This is an excitable phase slip, and as described above, such a slip often manifests as an amplitude pulsation. Various properties of the resulting distribution of interslip times are known for the Adler model. For the purposes of this work the most important feature is that the distribution has a broad peak from which it exponentially decays with a characteristic time T_K. Thus, for a weakly injected semiconductor laser one might expect to find such an interspike time distribution close to the locking boundary. However, as described above, to access such a region the injection is so weak that the intensity of the slave laser undergoes extremely small pulsations, and these can be below or similar to the perturbations due to noise in the time trace. Thus, one needs to directly access the phase where the excitable events are unambiguous as each one consists of a full 2π rotation regardless of the intensity variation. A technique to allow such a measurement has recently been developed, and we turn our attention to the experiment in the next section.

III. EXPERIMENT

For the experiment the master laser was a commercial tunable device with a linewidth <100 kHz, tunable in steps of at 0.1 pm, and the slave laser was a single mode (distributed feedback) quantum dot (QD) based device operating at approximately 1.3 μm, similar to those used in [21]. The setup

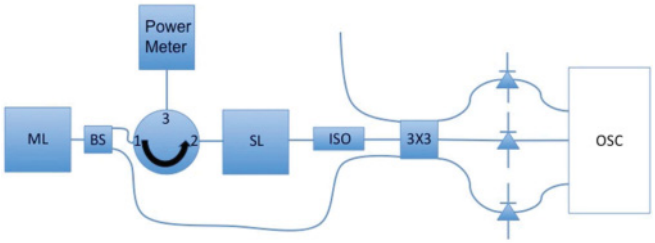

FIG. 1. (Color online) Experimental setup. ML is the master laser, BS is a beam splitter, SL is the slave laser, ISO is an optical isolator to prevent unwanted feedback, 3X3 is the passive 3 × 3 coupler, and OSC is the digital oscilloscope.

used the interferometric system described in [22], allowing experimental determination of the phasor of the slave electric field. The setup is shown in Fig. 1. The output from the master was split using a polarization maintaining beam splitter. The light from one arm of this splitter was coupled to the slave as injected light. The other arm of the splitter was connected to one arm of a passive 3 × 3 coupler. The output of the slave went to a second arm of the 3 × 3 coupler, while the final arm did not receive any input. The use of the optical circulator allows the output of the slave to be used as a reference for the coupling strength using the power meter. The three outputs from the 3 × 3 coupler were connected to a 14-GHz real-time digital oscilloscope. Any timing skew between the three outputs was removed. The outputs of the coupler have a fixed phase relationship, and through suitable combinations of the intensities one can calculate the phase of the slave laser in the frame of the master. Each output is phase dependent, while the sum may be phase independent. (See [22] for details.)

For sufficiently low values of the detuning between the master and slave frequencies the slave laser can be phase locked to the master. (We consider only negative detuning in this work.) We quantify the injection strength via the ratio of the intensity of the master field, which enters the slave cavity to the intensity in the slave's cavity in the injection-free case. In these units the injection strengths we consider are from 3×10^{-6} to 0.02. (To put this in perspective, levels greater than 0.1 are required for the observation of a Hopf bifurcation [21].) At the lowest levels considered, the change in intensity between the injection-free laser and the injection-locked laser is not clearly observable above the noise in the experiment, and the locking region is approximately 50 MHz wide. Figure 2 shows the intensity of the slave (plus a constant offset) in a regime where noise can excite phase slips. Also shown are the corresponding traces from the arms of the interferometer. The spike in each of these phase sensitive traces corresponds to a large phase excursion. Thus, the phase sensitive readings show that something significant is taking place in the phase, while the intensity is almost unchanged within the confines imposed by noise on the measurements. We resolve the phase of the slave in the frame of the master laser and find that the spikes correspond to a 2π rotation of the electric field. Figure 2 also shows the phasor for the rotation. The blue ("wiggly") line shows the experimental phasor of the slave laser. However, any variation in the intensity is almost entirely masked by the

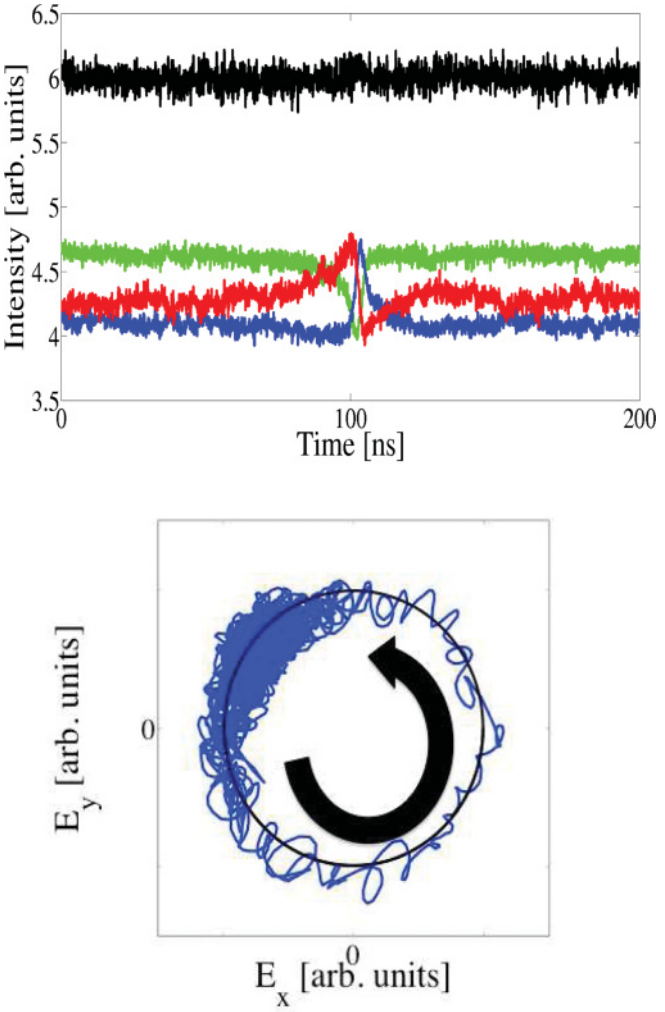

FIG. 2. (Color online) (top) The intensity of the slave undergoing extremely weak injection and the three outputs from the interferometer. The highest time series (black) is the intensity of the slave output, while the three lower traces (green, red, and blue, from top to bottom) with the sharp features are the outputs of the individual channels of the interferometer. The sharp features show that a large excursion is taking place in the phase, although the intensity is approximately constant (modulo noise). (bottom) The corresponding phasor plot. The dense part of the experimental (blue "wiggly" line) plot is the steady state position. The phase excursion is a 2π rotation and within the confines imposed by noise is approximately circular, as can be seen by comparing the trace with the (black) circle fitted using the steady state value to find the radius. The arrow shows the direction of rotation of the phasor during the excitable event.

noise, and so within the confines imposed by the experiment, the behavior is close to one-dimensional. To demonstrate how close it is to a circle we plot (in black) a circle with a radius given by the mean of the steady state intensity over a long time between two consecutive events. We note that much of the noise in the measurements is actually instrument noise, and so the identification of the pulsations may be significantly hampered by the measurement rather than the actual behavior of the slave laser.

The interspike statistics for a long time trace were analyzed, and a representative example of the histograms of interspike

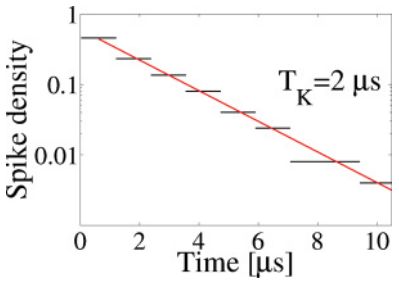

FIG. 3. (Color online) A histogram of interspike times for the weak injection case. The characteristic time T_K is also shown with the solid (red) line, showing the best fit exponential.

times is shown in Fig. 3 and yields an exponential decay. The characteristic time T_K of the exponential in the case shown is $2\mu s$. The identification and measurement of the phase rotations even when the intensity pulsation is almost entirely masked by the noise is one of our key results.

The effect on the intensity of increasing the injection strength is clear. The phase-locked intensity no longer even approximately matches the free-running intensity in general. For an injection strength of 0.01 clear intensity pulsations are already associated with the phase slips, and so the system is no longer even approximately one-dimensional. In Fig. 4 a train of such pulses is shown. A phasor plot of one pulse is also shown. From the intensity it is clear that the rotation cannot be on a circle, and the phasor confirms this directly. Indeed, the behavior is fully three-dimensional: that the carrier density also changes was confirmed by direct measurement by simultaneously measuring the gain of the slave laser using an extension of the phase technique as described in [22]. The corresponding distribution of interspike times is shown in Fig. 5. Again, there is an exponential tail (which becomes progressively steeper as the magnitude of the detuning is increased: that is, the Kramers time T_K decreases), but now there is also a sharp early peak over this tail. In this case the characteristic time of the tail is 67 ns, while the early peak is at approximately 6 ns. At this injection strength, the separation of time scales is also evident in the time series where the early peak is characterized by clusters of intensity pulses. These statistics are not consistent with the saddle-node, infinite period bifurcation as found in the Adler system. The signature on the statistics arising from the change of dimensionality in the system is another of our key results.

A noticeable contrast between the two injection levels is the influence of noise on the trajectory during the rotations shown in Figs. 2 and 4. For the low injection case each rotation takes a (relatively) long time. A full rotation occurs on a time scale of the order of tens of nanoseconds, and so the effect of noise can be easily seen in the trace and is manifest by the many loops and twists in the trajectory during the rotation. In the higher injection case a rotation occurs on the order of a nanosecond, and so the influence on the observed trajectory during a rotation is greatly decreased, and the trace is much sharper. The evolution from the exponential distribution to the nonexponential distribution is gradual, and there is no clear transition. Rather, an early peak develops and becomes progressively more prominent as the injection level is increased. In the time series one observes, in general,

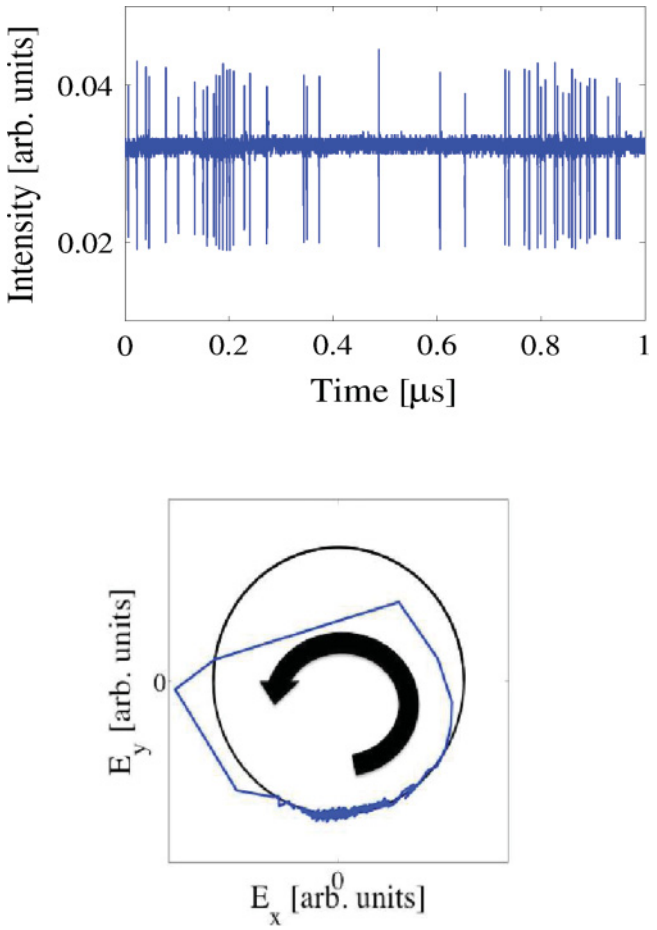

FIG. 4. (Color online) (top) An experimental pulse train. The injection strength was approximately 0.01. The detuning was approximately −0.25 GHz. (bottom) A phasor plot for one of the pulses. The dense part of the experimental (blue) plot is the steady state position. The phase excursion is a 2π rotation and is very noncircular, as can be seen by comparing the trace with the (black) circle fitted using the steady state value to find the radius. The arrow shows the direction of rotation of the phasor during the excitable event.

both individual isolated pulses and clusters of pulses. As the injection strength is decreased, the individual pulses dominate, and when it is increased, the clusters dominate.

To investigate the meaning behind the observations we use the machinery of laser rate equation models.

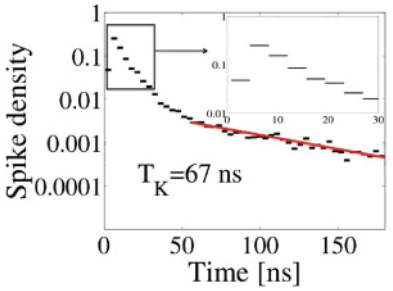

FIG. 5. (Color online) Experimental distribution of interspike times. The characteristic time T_K is shown with the solid (red) line, showing the best fit exponential for the tail. The inset shows a zoom of the peak in the histogram. The detuning and injection strength are the same as for Fig. 4.

IV. THEORY AND NUMERICAL SIMULATIONS

Let us take as our starting point the rate equations for an optically injected quantum dot laser.

$$E' = \frac{1}{2}(1+i\alpha)\left[1 - \frac{2(1+|E|^2)}{B\varepsilon N}\right]E + Ke^{i\Delta t}, \quad (2)$$

$$N' = \varepsilon^{-1}\eta[J - N - 2(1+|E|^2)]. \quad (3)$$

Here N is the carrier density in the wetting layer, $B \equiv \tau\tau_{\rm cap}^{-1}$, and $\eta \equiv \tau_{ph}\tau^{-1}$, where τ, $\tau_{\rm cap}$, and τ_{ph} denote the carrier recombination time, the capture time from the wetting layer to the dot, and the photon lifetime, respectively. J is the pumping current above threshold, and K is the injection rate. In these equations a prime means differentiation with respect to $s = \varepsilon t/\tau_{ph}$. The rate equations for a quantum dot laser usually include a further equation for the probability of occupation of the dot. Here we have adiabatically removed this equation, as described in [21,23]. While the full model can explain the observations, we derive a phase model valid for weak injection levels that allows the physics of the system to be more easily identified. Reductions to phase models have also been used in the mutually coupled (bidirectionally coupled) laser system [24,25] and to analyze mode hopping in semiconductor ring lasers [26], and such reductions can provide both accurate approximations and aid intuition, and this is also the case here. We consider the injection strength K to be very low so that $\kappa \equiv \frac{K}{R} \ll 1$, and we restrict the system to either be in or near the synchronized region, in which case the detuning must also be of order κ. We assume then that the resulting changes in the intensity and carriers are also of order κ. The derivation proceeds as follows. We write $E = Re^{i\phi+\Delta s}$. Equations (2) and (3) can then be rewritten as

$$R' = \frac{1}{2}\left[1 - \frac{2(1+R^2)}{B_1 N}\right]R + K\cos(\phi), \quad (4)$$

$$\phi' = -\Delta + \frac{\alpha}{2}\left[1 - \frac{2(1+R^2)}{B_1 N}\right] - \frac{K}{R}\sin(\phi), \quad (5)$$

$$N' = d[J - N - 2(1+R^2)], \quad (6)$$

where $B_1 = B\varepsilon$ and $d = \varepsilon^{-1}\eta$. Using Eq. (5) we can rewrite Eq. (4) as

$$R' = \frac{1}{\alpha}(\phi' + \Delta)R + K\frac{\sqrt{1+\alpha^2}}{\alpha}\sin(\phi + \phi_0), \quad (7)$$

where $\phi_0 = \arctan\alpha$. We assume now that $\kappa \equiv \frac{K}{R} \ll 1$. Then, we also assume that $R = R_{\rm f}(1+r)$, with $R_{\rm f}$ being the free-running value of R and $r \ll R_{\rm f}$, and that $N = N_{\rm f} + n$, with $N_{\rm f}$ being the free-running value of N and $n \ll N_{\rm f}$. To first order we find the following:

$$r' = \frac{1}{\alpha}(\phi' + \Delta) + \kappa\frac{\sqrt{1+\alpha^2}}{\alpha}\sin(\phi + \phi_0), \quad (8)$$

$$\phi' = -\Delta + \frac{1}{2}\alpha\left[\frac{n}{N_{\rm f}} - \frac{4R_{\rm f}^2 r}{B_1 N_{\rm f}}\right] - \kappa\sin\phi, \quad (9)$$

$$n' = -d\left[n + 4rR_{\rm f}^2\right]. \quad (10)$$

Rearranging Eq. (9), we can write n in terms of ϕ',ϕ, and r. Differentiating this, we find

$$n' = N_f\left[\frac{2}{\alpha}(\phi'' + \kappa\phi'\sin\phi) + \frac{4R_f^2 r'}{B_1 N_f}\right]. \tag{11}$$

Now, here we implement our slow phase approximation. We are only interested in the behavior near or in the locking region, and so we restrict the detuning to be of order κ. Then from Eq. (9), ϕ' is also of order κ, and so, in the last expression, the term involving $\kappa\phi'$ can be ignored to first order. Substituting for r', equating with the right hand side of Eq. (10), and differentiating, we find

$$\phi''' + 2\Gamma\phi'' + \Omega^2[\phi' + \Delta + \kappa\sqrt{1+\alpha^2}\sin(\phi+\phi_0)] = 0, \tag{12}$$

where

$$\Gamma = \tfrac{1}{2}(d + 1 - J_{th}/J) \tag{13}$$

and

$$\Omega^2 = d(1+B_1)[1 - J_{th}/J], \tag{14}$$

where J_{th} is the threshold current, Γ is the relaxation oscillation damping, and the relaxation oscillation frequency is given by $\sqrt{\Omega^2 - \Gamma^2}$ [23]. Finally, dividing across by Ω^3 and rescaling the time so that a dot means differentiation with respect to Ωs, we find

$$\dddot{\phi} + 2\widehat{\Gamma}\ddot{\phi} + \dot{\phi} + \chi\,\sin(\phi+\phi_0) + \widehat{\Delta} = 0, \tag{15}$$

where $\widehat{A} \equiv \frac{A}{\Omega}$ and $\chi = \widehat{\kappa}\sqrt{1+\alpha^2}$. Defining $\psi = \phi + \phi_0$, we can rewrite this equation as

$$\dddot{\psi} + 2\widehat{\Gamma}\ddot{\psi} + \dot{\psi} + \chi\,\sin\psi = -\widehat{\Delta}, \tag{16}$$

so that it now resembles clearly a generalization of the forced nonlinear pendulum to a third-order system. This equation can also be derived for quantum well (QW) lasers using the same approximations, and so it provides a quasicanonical form for weakly injected semiconductor lasers within the slow phase region [27]. It is also a natural generalization of both the Adler equation and the forced nonlinear pendulum to three dimensions and as a result should be of interest to researchers in diverse fields. The ratio of the damping Γ and the frequency Ω is a crucial parameter in our system. For quantum dot lasers this can be of order unity, while for conventional QW lasers $\Gamma << \Omega$, with the result that there are large regions of chaotic operation [28]. For our numerical simulations, we take $\widehat{\Gamma}$ to be 0.8 for the quantum dot laser operating at 1.5 times threshold.

There are two main bifurcations associated with this equation. The first is a saddle-node (SN) bifurcation, and the second is a homoclinic bifurcation. The SN bifurcation corresponds to the locking boundary and the creation of a phase-locked solution, while the homoclinic corresponds to the death of the running-phase solution. As described earlier, for the Adler system the two bifurcations coincide, forming a saddle-node infinite period bifurcation. However, in the three-dimensional system, they do not always coincide. Rather, above a critical value of the injection strength the homoclinic bifurcation is located inside the locked region, and so there is a region of bistability between a stable locked steady state and the running-phase solution. (This bistability is quite different to that described in [21], where a bistability results from the interaction of SN and Hopf bifurcations.) A bifurcation diagram is shown in Fig. 6. The solid (blue) line shows the saddle-node bifurcation, and the dashed (red) line shows the homoclinic. The first realization that a separation between the saddle-node and homoclinic bifurcations can occur in the optically injected system was in [6], where weakly damped quantum well lasers were considered. There it was shown that a separation could lead to complicated multipulse excitability in so-called homoclinic teeth. We see now that for highly damped lasers such as the QD laser used in our experiment, a separation between the two bifurcations also arises, but in this case it leads to a bistability between phase-locked behavior and an unlocked limit cycle rather than the complicated multipulse excitability. It is this bistability that is responsible for the nonexponential distributions. In [23] it was shown that the low damping in quantum well lasers leads to chaotic regions associated with the homoclinic teeth and that the high damping of quantum dot lasers removes these chaotic regions and the corresponding teeth. We will see here that the phase model allows the identification of the physical mechanism responsible for the bistability in the highly damped system. First, let us consider some numerically generated time series.

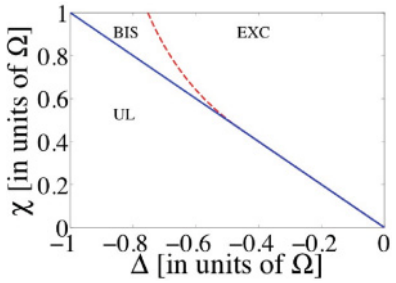

FIG. 6. (Color online) Bifurcation diagram for Eq. (15). The solid (blue) line is the saddle node, and the dashed (red) line is the homoclinic. UL, BIS, and EXC are unlocked, bistable, and excitable, respectively.

To obtain noise-induced pulses and bistable switching, a white noise term $\sqrt{2D}\xi(T)$, with $\langle\xi(T),\xi(T')\rangle = \delta(T - T')$, was added to Eq. (15). From numerical time series of the data one can examine the interspike time distributions. (Some considerations of numerically generated interspike time distributions in optically injected QW lasers were presented in [29].) In the excitable region and far from the homoclinic bifurcation, the distributions are close to exponential, but as the homoclinic bifurcation is approached, an early peak develops and becomes increasingly prominent, although there is always

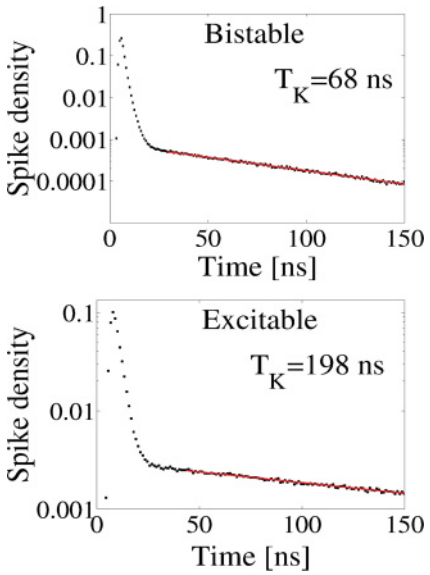

FIG. 7. (Color online) Numerical distributions. (top) The system is in the bistable region, and the parameters are $\chi = 1$ and $\Delta = 0.9$. (bottom) The system is in the excitable region, and the parameters are $\chi = 0.8$ and $\Delta = 0.67$. $D = 0.036$ and $\widehat{\Gamma} = 0.8$ for both plots.

an exponential tail. In the bistable region the distributions are also of this shape, with the early peak becoming increasingly sharp. Two examples of the numerical histograms generated are shown in Fig. 7. For the first distribution, the parameters were chosen to match the experimental situation illustrated in Fig. 4. With these parameters the theoretical system is in the bistable region. The agreement with the experiment is excellent. For the second histogram the system is explicitly in the excitable region, and yet the early peak is still clearly visible, although there is no deterministic frequency. Thus, this early peak is a noisy precursor of the homoclinic bifurcation [30]. A similar effect in semiconductor ring lasers was recently analyzed in [26] for bistable switching but in a system where the dimensionality was fixed. The histograms in the two regions are qualitatively similar, and this leads to a problem identifying the boundary of bistability. In an idealized, noise-free system one can easily identify the boundary between the excitable region and the bistable region, as in the bifurcation picture of Fig. 6. For example, one could sweep the detuning from the phase-locked region through the bistable region and into the unlocked region and then reverse the sweep direction and thereby find the boundaries. However, in the real system, noise obscures these boundaries. This was also clear in the experimental case. This ambiguity is particularly prominent in a situation where the region of bistability is small.

V. REDUCTION TO TWO-DIMENSIONAL SYSTEM

We note that in certain circumstances Eq. (12) can be simplified even further, yielding a second-order phase equation formally identical to that of the forced nonlinear pendulum. To derive the second-order equation there are two possible routes. The first is to take the Class A approximation [31,32], where both Γ and Ω are much greater than 1 (usually because of the inherent time scales in the device). Then one can neglect the third-order term in Eq. (12) and find the following second-order equation:

$$\phi'' + \frac{\Omega^2}{2\Gamma}[\phi' + \chi\ \sin(\phi + \phi_0) + \Delta] = 0. \tag{17}$$

A second route is to take J to be only slightly above J_{th}. This is interesting as it is independent of the inherent time scales in the device, unlike the usual Class A system. As J approaches J_{th}, Ω approaches zero while Γ remains finite and approaches $\frac{1}{2}d$. Then Eq. (12) becomes

$$\phi''' + 2\Gamma\phi'' = 0. \tag{18}$$

Integrating this and demanding consistency with the low injection Adler limit, we find

$$\phi'' + 2\Gamma\phi' = -2\Gamma[\Delta + \kappa\sqrt{1+\alpha^2}\ \sin(\phi + \phi_0)]. \tag{19}$$

In both of these cases we can write the equation as

$$\psi'' + 2\gamma\psi' + \omega^2\ \sin\psi = F, \tag{20}$$

which is formally identical to that of the forced nonlinear pendulum, by employing a suitable relabeling and defining γ and F appropriately. This reduction from a three-dimensional system to a two-dimensional system preserves the existence of excitable and bistable regimes separated by a homoclinic bifurcation, and a similar effect is observed close to this bifurcation [33]. We note that in both of these cases one could begin with the rate equations and justify an adiabatic elimination of the carrier equation. This would lead to a two-dimensional system from which the second-order phase equation could be found via the weak injection and slow phase approximations.

VI. TILTED WASHBOARD POTENTIAL

A standard physical analogy is to consider a particle in the tilted washboard potential. In the infinite friction limit of the forced nonlinear pendulum one recovers the Adler system. This is amenable to analysis using Fokker-Planck methods, and many of the results are well known [34,35]. For finite friction one recovers the standard forced pendulum [and our Eq. (20)] where now, as well as the velocity, the equation of motion depends on the acceleration of the phase, and this is also treated in [35] (but from a different point of view to our treatment in this work). Finally, if as well as phase acceleration one has *jerk* of the phase (the derivative of the acceleration), then one arrives at our full three-dimensional equation. In each case the potential is of the same general form:

$$V(\phi) = T\phi - S\cos(\phi), \tag{21}$$

where T provides the tilt (and is analogous to the detuning), and the value of S relative to T corresponds to the depth of the minima (and is analogous to the injection strength). In all cases, phase locking corresponds to the particle residing at a local minimum of the potential. In the infinite friction Adler case this is the only stable solution when the minima exist. The introduction of higher derivatives of the phase allows very different dynamics. When these are introduced, given appropriate initial conditions, one can also find a solution where the particle runs down the potential even in the presence of the local minima.

The creation of this running-phase solution corresponds to the homoclinic bifurcation. This allows a physical picture of the generation of the bistability. The running-phase solution essentially amounts to throwing the particle quickly enough down the potential to overcome the friction and the attraction of the potential minima. Phase-locked behavior corresponds to a stationary solution in one of the potential minima. In the presence of noise one can find switching between these two behaviors.

VII. CONCLUSION

We have presented a phenomenon hitherto unobserved in the optically injected semiconductor laser, a scientifically and technologically important system. Specifically, we showed that depending on the injection strength, the noise-induced excitability can show markedly different statistics. For extremely low injection strengths the system is effectively one-dimensional, and the interspike distribution resembles an exponential decay, while for increasing injection strength, the system becomes three-dimensional and an early peak develops in the distribution. In the low injection strength case a novel technique was required to identify the excitable events as the intensity pulsations are masked by the noise at such low levels, and so the phase of the slave laser has to be directly measured to identify the rotations. Generic phase equations were derived generalizing the Adler equation. The experimentally relevant equation reproduced the experimental distributions identifying the emergence of the early peak with the presence of a homoclinic bifurcation.

ACKNOWLEDGMENTS

This work was conducted under the framework of the INSPIRE programme, funded by the Irish Government's Programme for Research in Third Level Institutions, Cycle 4, National Development Plan 2007-2013 and the authors also gratefully acknowledge the support of Science Foundation Ireland under Contract No. 07/IN.1/I929. The authors in Bruxelles acknowledge the support of the Fonds National de la Recherche Scientifique (Belgium). The research by T.E. was also supported by the Air Force Office of Scientific Research (AFOSR) grant FA8655-09-1-3068.

[1] A. L. Hodgkin and A. F. Huxley, J. Physiol. **117**, 500 (1952); R. FitzHugh, Biophys. J. **1**, 445 (1961); J. Nagumo, S. Arimoto, and S. Yoshizawa, Proc. IREE Aust. **50**, 2061 (1962).

[2] B. Lindner, J. García-Ojalvo, A. Neiman, and L. Schimansky-Geier, Phys. Rep. **392**, 321 (2004).

[3] F. Plaza, M. G. Velarde, F. T. Arecchi, S. Boccaletti, M. Ciofini, and R. Meucci, Europhys. Lett. **38**, 85 (1997).

[4] M. Giudici, C. Green, G. Giacomelli, U. Nespolo, and J. R. Tredicce, Phys. Rev. E **55**, 6414 (1997).

[5] H. J. Wünsche, O. Brox, M. Radziunas, and F. Henneberger, Phys. Rev. Lett. **88**, 023901 (2001).

[6] S. Wieczorek, B. Krauskopf, and D. Lenstra, Phys. Rev. Lett. **88**, 063901 (2002).

[7] D. Goulding, S. P. Hegarty, O. Rasskazov, S. Melnik, M. Hartnett, G. Greene, J. G. McInerney, D. Rachinskii, and G. Huyet, Phys. Rev. Lett. **98**, 153903 (2007); B. Kelleher, D. Goulding, S. P. Hegarty, G. Huyet, Ding-Yi Cong, A. Martinez, A. Lemaître, A. Ramdane, M. Fischer, F. Gerschütz, and J. Koeth, Opt. Lett. **34**, 440 (2009).

[8] O. Vaudel, N. Péraud, and P. Besnard, Proc. SPIE **6997** 69970F (2008).

[9] L. Gelens, L. Mashal, S. Beri, W. Coomans, G. Van der Sande, J. Danckaert, and G. Verschaffelt, Phys. Rev. A **82**, 063841 (2010).

[10] D. Sigeti and W. Horsthemke, J. Stat. Phys. **54**, 1217 (1989).

[11] Hu Gang, T. Ditzinger, C. Z. Ning, and H. Haken, Phys. Rev. Lett. **71**, 807 (1993).

[12] W.-J. Rappel and S. H. Strogatz, Phys. Rev. E **50**, 3249 (1994).

[13] A. S. Pikovsky and J. Kurths, Phys. Rev. Lett. **78**, 775 (1997).

[14] H. Kramers, Physica (Utrecht) **7**, 284 (1940).

[15] P. Hänggi, P. Talkner, and M. Borkovec, Rev. Mod. Phys. **62**, 251 (1990).

[16] P. Reimann, C. Van den Broeck, H. Linke, P. Hänggi, J. M. Rubi, and A. Pérez-Madrid, Phys. Rev. E **65**, 031104 (2002).

[17] S. Wieczorek, B. Krauskopf, T. B. Simpson, and D. Lenstra, Phys. Rep. **416**, 1 (2005).

[18] R. Adler, Proc. IRE **34**, 351 (1946); reprinted in Proc. IEEE **61**, 1380 (1973).

[19] T. Erneux and P. Glorieux, *Laser Dynamics* (Cambridge University Press, Cambridge, 2010).

[20] S. H. Strogatz, *Nonlinear Dynamics and Chaos* (Addison-Wesley, Reading, MA, 1994).

[21] T. Erneux, E. A. Viktorov, B. Kelleher, D. Goulding, S. P. Hegarty, and G. Huyet, Opt. Lett. **35**, 937 (2010).

[22] B. Kelleher, D. Goulding, B. Baselga-Pascual, S. P. Hegarty, and G. Huyet, Eur. Phys. J. D **58**, 175 (2010).

[23] B. Kelleher, C. Bonatto, G. Huyet, and S. P. Hegarty, Phys. Rev. E **83**, 026207 (2011).

[24] H.-J. Wünsche, S. Bauer, J. Kreissl, O. Ushakov, N. Korneyev, F. Henneberger, E. Wille, H. Erzgräber, M. Peil, W. Elsäßer, and I. Fischer, Phys. Rev. Lett. **94**, 163901 (2005).

[25] B. Kelleher, C. Bonatto, P. Skoda, S. P. Hegarty, and G. Huyet, Phys. Rev. E **81**, 036204 (2010).

[26] S. Beri, L. Gelens, M. Mestre, G. Van der Sande, G. Verschaffelt, A. Scirè, G. Mezosi, M. Sorel, and J. Danckaert, Phys. Rev. Lett. **101**, 093903 (2008).

[27] We note that this equation was also derived in A. Gavrielides, V. Kovanis, P. M. Varangis, T. Erneux, and G. Lythe, Quantum Semiclass. Opt. **9**, 785 (1997) for quantum well lasers but under the assumptions of large α and low RO damping, rather than a slow-phase approximation. We use the slow-phase

approximation here as it removes any dependence on the material properties.

[28] V. Kovanis, A. Gavrielides, and J. A. C. Gallas, Eur. Phys. J. D **58**, 181 (2010).

[29] S. Wieczorek and D. Lenstra, Phys. Rev. E **69**, 016218 (2004).

[30] K. Wiesenfeld, J. Stat. Phys. **38**, 1071 (1985); A. Neiman, P. I. Saparin, and L. Stone, Phys. Rev. E **56**, 270 (1997).

[31] F. T. Arecchi, G. L. Lippi, G. P. Puccioni, and J. R. Tredicce, Opt. Commun. **51**, 308 (1984).

[32] C. Mayol, R. Toral, C. R. Mirasso, and M. A. Natiello, Phys. Rev. A **66**, 013808 (2002).

[33] M. C. Eguia and G. B. Mindlin, Phys. Rev. E **61**, 6490 (2000).

[34] R. L. Stratonovich, *Topics in the Theory of Random Noise* (Gordon and Breach, New York, 1963).

[35] H. Risken, *The Fokker-Planck Equation* (Springer, Berlin, 1984).